Solid State NMR Probe Design

F. David Doty
Doty Scientific Inc., Columbia, SC, USA

1 INTRODUCTION

The majority of solids NMR experiments today are driven by biological applications in rigid macromolecules, where even the most advanced liquids methods are limited by the spectral resolution they can achieve.[1] Obtaining detailed structural information from NMR of solid samples is often more technically demanding than for liquids because of the absence of molecular tumbling in solids to average line-broadening interactions; hence, much greater probe bandwidths are required.[2-4] A wide array of line narrowing techniques have been developed over the past twenty years for solid samples that greatly extend the earlier capabilities.[1]

The original solids probe, the wideline probe, usually has spectral excitation bandwidth greater than 80 kHz (i.e., able to generate 90^0 pulses less than 3 μs). To do this, it normally must withstand peak rf voltages in excess of 2 kV – possibly up to 5 kV. Often wideline probes are double-tuned (DT) to permit cross polarization (CP) and high-power decoupling for increased sensitivity and resolution. Multiple-pulse line-narrowing techniques may be used to remove dipolar broadening, especially if π/2 pulse lengths below 2 μs can be generated. At very high fields, this is more readily achieved in single-resonance probes, where coils of very low inductance can be used effectively.

The Cross-Polarization/Magic Angle Spinning (CPMAS) probe adds high-speed sample spinning at the Magic Angle to the other capabilities of the DT wideline probe for effective averaging of susceptibility broadening, chemical shift anisotropy, and often dipolar broadening, thereby greatly improving resolution for most spin-1/2 nuclei.[5] The 3D spectral capabilities of a triple resonance probe, especially $^1H/^{13}C/^{15}N$, are extremely useful in solving structures of larger molecules. Hence, the triple-resonance MAS probe is quickly becoming the most commonly used solids probe in macromolecule applications.[6] In many cases, spinning rates above 20 kHz, decoupling field strengths above 100 kHz with low rf heating of the sample, very high sensitivity on all three channels, high spectral resolution, and wide variable temperature (VT) range with stable control are important. In some cases, it is also desirable to be able to apply a $\boldsymbol{B}_0$ gradient at the magic angle and have automatic sample exchange capability. The combination of these features makes such a probe a technically challenging instrument.[7]

When sufficiently large single crystals of the sample can be grown, high-resolution spectra and the chemical shift tensor can be obtained using a single-crystal probe,[8] which is similar to a wideline probe but includes a goniometer and crystal orientation mechanism for rotating the sample, possibly about three perpendicular axes. Related methods may be applied to the study of membrane proteins that are highly oriented by any of a number of different techniques, and such studies have recently become more widely used, especially using the PISEMA technique.[9]

Naturally, some of the solids NMR techniques that seemed quite promising 10 to 20 years ago have been superseded, but novel applications continue to be explored for many of the specialized techniques, such as Magic Angle Turning (or ultra-slow MAS), Dynamic Angle Spinning (DAS), Double Ro-

tation (DOR), and single crystals. However, the primary thrust of current solids NMR probe development is improved S/N with small samples (2-60 μL) of biological macromolecules. To this end, current probe developments include (1) cryogenic cooling of tuning elements other than the sample coil in triple-resonance MAS with 2-4 mm rotors in narrow-bore magnets,[10] (2) cryogenic cooling of all coils and capacitors in triple-resonance 3 mm MAS in wide-bore magnets,[11] (3) 1.3 mm MAS with up to 70 kHz spinning rate,[12] (4) SAS at very high fields in narrow-bore magnets,[13] and (5) higher power triple-resonance probes for oriented samples with minimal decoupler heating.[14] Unlike in MRI and low-field liquids NMR probes, the performance of state-of-the-art solids probes is usually significantly limited by the capacitors.[6, 7, 11, 15]

2 HIGH-POWER CAPACITORS

The special requirements of capacitors for NMR probes include the following: ultra-low magnetic susceptibility, high Q, high voltage, high current, ultra-low piezoelectric effects, high stability with temperature changes, and dielectrics devoid of unwanted NMR background signals. Losses in rf capacitors at a given frequency may be indicated by a capacitor quality factor Q_c, an effective series resistance [ESR=$(\omega C Q_c)^{-1}$], a loss tangent ($\tan\delta \cong \pi/Q_c$), or a loss factor, $k_d \tan\delta$, where k_d is the dielectric constant (relative permittivity). Direct current (DC) losses may be specified by a leakage resistance, but this usually has no relationship to R_P (the effective parallel resistance of a tuned circuit) above ~5 MHz.

Solids probes are usually designed for peak rf voltages of 2 to 5 kV, compared to 1 to 2 kV for most liquids probes. Voltage breakdown strengths often tabulated for dielectrics are best ignored unless two important parameters are also specified: test material thickness and frequency. The frequency dependence is not easily characterized, but DC ratings of rf capacitors are typically four times the short-pulse rf ratings at 100 MHz. For very short pulses where heating is not much of a factor, the voltage rating at 10 MHz is typically only twice that at 500 MHz, but with long pulses the voltage often derates as the 3/2 power of frequency above a cutoff that is a function of Q_c/C. Table 1 shows typical rf breakdown voltages, V_B, for several thicknesses of low-k and high-k dielectrics at 30 MHz. Above 50-100 V, V_B is a square root function of thickness and shows relatively little variation within the two classes of rf dielectrics listed.[16] Dry air has ionization V_B comparable to that of high-k dielectrics, but arc voltage in monatomic gases (He, Ne, Ar) is less by a factor of at least five (more for large gaps) because of the absence of low-energy rotational and vibrational relaxation modes.[17] The additional rotational modes in polyatomic gases usually increase the breakdown voltage, except in the case of ionic gases such as H_2O.

Table 1 Typical Dielectric Breakdown Voltages at 300 MHz

Thickness (mm)	V_B, for $k_d > 30$ (V)	V_B, for $k_d < 10$ (V)
0.1	500	1000
0.5	1200	2200
3.0	3000	5400

2.1 Ceramic Capacitors

The stable COG (ceramic oxide glass) rf capacitor specification (type NPO) requires temperature coefficient less than ±30 ppm and $\tan\delta$ below 0.001 for the range -55 to 125^{0}C. For moderate-power applications up to 300 MHz, the COG formulation often consists of fine-grained baria-neodymia-titania systems or magnesium titanate prefired with 6 mol% calcium titanate, but they are also made from mixtures of neodymium carbonate, titania, and barium titanate.[18] A two-stage firing is generally required for multilayer capacitors so that the final firing temperature can be kept below 1120^{0}C (preferably even below 1070^{0}C) to allow the use of Pd-Ag electrodes.[19] The ceramic precursors are prefired at high temperature, then re-ground and mixed with a powdered glass binder with matched thermal expansion such as 36%

CdO, 23% Bi_2O_3, 25% PbO, 5% ZnO, 5% B_2O_3, 5% SiO_2, 1% Al_2O_3.[20] Alternate layers of ceramic/glass and metallization slurry are built up by a screening or spraying process.

Porcelains (mostly magnesium-aluminum-silicates with up to 10% glass phase) are often used in the UHF range for high-power capacitors below 15 pF. Corning Pyroceram 9606 consists mostly of cordierite ($2MgO\text{-}2Al_2O_3\text{-}5SiO_2$), with lesser amounts of cristobalite and various magnesium titanates. Its low thermal expansion can cause problems with the metallization. Forsterite ($2MgO{\cdot}SiO_2$) is electrically almost as good as pyroceram, easier to produce, and easy to metallize, but has poor thermal shock resistance. These ultra-low-loss formulations typically have a positive temperature coefficient (the capacitance increases ~90 ppm/^{0}C), which can exacerbate spectral artifacts in some 2D indirect-type experiments demanding ultra-stable phase, Q, and matching.

UHF high-power capacitors above 30 pF are often based on strontium titanate, which is not piezoelectric but may contain piezoelectric barium titanate impurities. High-power rf capacitors are often coated with a sealing glass such as $2PbO{\cdot}SiO_2$ (550^{0}C) to keep out moisture,[20] as it facilitates silver migration in the presence of an electric field. A number of manufacturers (including JFD, ATC, TEMEX, Murata, and Johanson) offer 3-kV multilayer ceramic rf capacitors in roughly a 3.5 x 10 x 11 mm^3 package. The JFD and Murata capacitors usually have the highest Q_C, but the differences are small. A reasonable estimate of the quality factor of a low-loss ceramic capacitor of capacitance C_P picofarads at f_0 MHz is given by the following:

$$Q_C \approx 1.5E07\, C_P^{-0.85} f_0^{-1.35} \qquad (1)$$

For example, the Q_C of a 10 pF capacitor at 600 MHz is typically about 350. However, there is usually a substantial spread (often $\pm$25%) in Q_C within a batch, and it can be worth the effort to select capacitors for critical applications using a special test fixture.

Perhaps 1% of new capacitors may initially be noisy in a high-power double resonance circuit, possibly as a result of micro-gaps between the electrodes or terminations and the dielectric,[21] and perhaps another 0.5% will become noisy within the first few hours of high-power operation. Premature breakdown may be initiated by surface tracking and moisture in solder rosin.

The magnetic properties of ceramic capacitors are unpredictable, as many ceramics are slightly diamagnetic (bismuth compounds are very diamagnetic), palladium is extremely paramagnetic, and ferromagnetic nickel barriers are used in the standard terminations, though Pd-Ag and sometimes copper are available on special order. The ceramic formulations continue to evolve, and many of the variations have included paramagnetic and ferromagnetic additions.[18, 22]

A number of manufacturers are by now somewhat familiar with the requirements of NMR/MRI capacitors and offer "non-magnetic" chip capacitors (no nickel) with 500–1500 V rating in a 2.2-3 mm cube, but it is always necessary to screen them for magnetism using a small magnet (a 2-mm cube of high-energy neodymium-boron-iron) suspended from a string. However, this is not sufficiently sensitive to detect bulk volumetric susceptibility χ_V (in SI units) below ~80 ppm – an order of magnitude beyond what is sometimes acceptable, even in a solids probe, if located within ~8 mm of the sample coil. For example, we have recently found (by NMR testing) the bulk susceptibility of some Cornell Dublier MCN non-magnetic capacitors to be 32 ppm. The current ATC 700B series (NPO) chip capacitors (termination TN, "non-magnetic") have bulk susceptibilities in the range of 20-25 ppm for capacitors ranging from 2.7 pF to 13 pF respectively. The magnitude of the bulk susceptibility of the TEMEX CHB series (temperature coefficient of 90 ppm/^{0}C), which have slightly better voltage handling and loss characteristics, seems to be below 3 ppm for a similar range of values. However, the ATC 700B series are often preferred because of their improved thermal stability and reliability at high temperatures.

2.2 Piezoelectric Acoustic Ringing

While acoustic ringing is seldom a problem in liquids probes because of the longer T_2s and the effectiveness of the acoustic suppression sequences, acoustic ringing of capacitors can obscure signals in solids probes requiring very short recovery times.[15, 23] Subjecting a capacitor with ferroelectric impurities

to a DC electric field in excess of 1 kV/mm, as may occur in a voltage withstanding test or from asymmetric rf breakdown, causes domain alignment and imparts a net crystallographic piezoelectric orientation to the ceramic. The ferroelectric is said to be "poled", and may exhibit acoustic ringing, even at zero field. The polarization of ferroelectrics can be annealed out by heating above the Curie temperature (130 ^{0}C for $BaTiO_3$; 180-300 ^{0}C for lead-magnesium-niobates), but they can easily become poled again.

Grain size is usually under 4 μm for rf power COG capacitors in the 10-30 pF range, in which case Raleigh scattering will normally keep acoustic decay times under a few μs above 30 MHz. However, grain size may exceed 100 μm in high-voltage (HV) capacitors above 150 pF and occasionally in low-valued capacitors, resulting in reduced acoustic absorption and acoustic decay times greater than 10 μs at surprisingly high frequencies.

Virtually all high-performance ceramic rf capacitors available today are specified by the manufacturer as having zero piezoelectric effect – but that does not mean they will not exhibit acoustic ringing at some surprisingly high frequencies in high magnetic fields. The Lorentz interaction is seldom a problem in driving acoustic modes in bulk metals (other than aluminum) above 15 MHz.[24] However, the Lorentz interaction can fairly often drive acoustic modes in multi-layer ceramic capacitors. While our experience is that acoustic modes in capacitors are uncommon above 50 MHz, Gorkov et al have reported some ATC 100B capacitors ringing for as much as 200 μs at 60 MHz in a 14 T field.[15] It is probably hopeless to attempt to explain these acoustic resonances in detail (but the acoustic wavelength at 30 MHz is ~0.1 mm, and electrode thicknesses may be comparable to lambda/2). The ringing is generally eliminated by changing the offending capacitor to one from a different series or perhaps to two in parallel. The difficulty can be in identifying the culprit.

2.3 Variable Capacitors

The XVT CPMAS probe shown in Figure 1 illustrates the use of two common types of variable capacitors, quartz dielectric and pressurized gas, in an MAS probe with Magic Angle Gradient (MAG) coils around the spinner assembly.

Figure 1 An MAS probe with a magic angle gradient coil (Doty Scientific, Inc.)

Perhaps the single component most synonymous with solids NMR probes is the Jennings CHV1N-45 gas variable capacitor – with its 22-mm diameter ceramic cylindrical insulator.[25] The capacitor is pressurized with about six atmospheres of gas (probably mostly SF_6, which has 8 times the dielectric strength of air) in its minimum capacitance position and may be adjusted from 1.5 to 45 pF using a pushrod mechanism. They come with rated peak voltage breakdown V_B up to 7.5 kV, though we've never confirmed more than ~4.5 kV near the low-end of the capacitance range, where the gas is less com-

pressed. The ceramic-to-metal seals are slightly magnetic, but this is seldom a problem as they are normally more than 20 mm from the sample. These variables have been used successfully for tuning purposes at least up to 220 MHz. They are usable from -20^{0}C to 100^{0}C and generally tolerate repeated over-voltages. However, if the external mechanical stop is not set properly, they may be easily damaged by pushing the adjustment rod beyond the specified limit. Also, they may leak slowly and thus go bad over time, and we have seen some fail initially at low voltages even without evidence of a loss of pressure (possibly from internal burrs).

The Johanson 5000-series nonmagnetic, air-dielectric, trimmer capacitors are commonly used in liquids NMR probes, and they can also be used on the high frequency (HF) channel in solids probes with capacitive voltage division. This capacitor consists of an alumina ceramic housing supporting several concentric, silver plated brass cylinders at the 'hot' end; a precision screw mechanism adjusts a similar intermeshing arrangement at the mount end. The minimum radial air gap is under 0.1 mm, and breakdown occurs at 500-700 V when new. With use, alignment deteriorates, and the voltage rating decreases. Care must be taken to avoid dissolving the internal lubricants (which are essential for acceptable lifetime) with cleaning solvents. The capacitors may be sealed, but this is inconvenient; hence, their voltage rating also decreases with altitude and humidity or high concentrations of monatomic gases. These variable capacitors are manufactured using 290^{0}C Pb-Sn-Ag solder between the alumina and brass body parts, and they tolerate repeated over-voltages without permanent damage.

The 2.5-kV rf capability of the JMC 7584, quartz-dielectric, 0.8-10 pF, variable capacitor (one is partially visible on the left side in Figure 1) usually allows more than an order of magnitude more tuning range than the small 1-10 pF air variables, as tuning range is often proportional to CV^2. Defective silver plating on the piston or sleeve has occasionally been found to produce noise at lower voltages in double-resonance circuits.[21] Impurities in the brass base and piston of the JMC capacitor may not be controlled as carefully as in a similar capacitor by Voltronics, but the JMC capacitor is mechanically much more robust,[21] which simplifies certain capacitive voltage division arrangements,[26] and the magnetism is not significantly different from the Voltronics version. These capacitors have been used successfully (at the lower end of their adjustment range) up to 500 MHz, even though their series inductance is 8-12 nH, depending on how they are mounted. Moreover, it is not difficult to disassemble and shorten them (reducing their range to 1-7 pF) so that they work well up to 600 MHz. They may lock up at high temperatures from the piston expanding or at low temperatures from the lubricants freezing, but the beauty of this capacitor is that, like the air and gas capacitors, it is usually not damaged by breakdown during a short pulse.

Teflon variables with low magnetism are available from Polyflon and Voltronics in a variety of sizes and ratings similar to the three described above, but teflon does not tolerate the brief, inadvertent over-voltages which are unavoidable in most laboratories using solids NMR probes. However, teflon tuning slugs in transmission lines have proven quite effective as long as the voltage limits are respected.[6]

3 SAMPLE COILS FOR SOLIDS

Prior to 1997, almost all solids probes used a single, transverse, solenoidal rf coil, irrespective of the frequency and number of channels, as the solenoid has considerably higher $Q\eta_f$, where η_f is the filling factor, over a very wide range of conditions.[27] In larger coils, optimum space between wires is half the wire diameter,[27] though in microcoils it is much less.[28] An enamel coating does not usually cause a background problem with carbon experiments, but it should be removed using warm sulfuric acid if proton experiments are planned.

High-Q circuits are usually preferred – except in some wideline applications. Coil length-to-diameter ratio is not critical, but values between 1.4 and 2.5 are usually best. Coil forms help stabilize tuning but reduce both filling factor and maximum voltage before the onset of arcing. If used, they should be of low-permittivity dielectrics to minimize arcing problems.

Special or custom wire may be obtained from MWS Wire Industries, Westlake Village, CA.

Gold flash (0.3-μm plating) is often applied to prevent copper sulfates and chlorides (which have large positive susceptibility due to antiferromagnetism) from forming on the wire surface, but it is critical to specify that the common practice of first applying a nickel strike (to minimize diffusion into the copper) be omitted or the wire will be very magnetic. The gold flash degrades the Q by about 1%. Silver plating does not improve Q (because of unavoidable defects) and does not provide the same degree of protection against corrosion – even when the plating thickness is increased to 3 μm.

Applications for high-resolution MAS of semi-solids began to appear in the early 1990's,[29] and it became clear that the much more attention needed to be given to improving B_0 homogeneity in solids probes.[30-32] Copper coils in high-resolution liquids probes are often plated with the proper thickness of palladium or rhodium to cancel the diamagnetism of copper,[33] and the required plating thickness is thin enough that Q is not degraded enough to matter. However, a better approach for heavy wire, as is needed in high-power solenoids for solids, is aluminum-core copper wire. This is available from a probe manufacturer in a range of sizes with bulk susceptibility below 3% that of pure copper.[34] Triple-resonance high-power MAS probes using such wire have demonstrated under 0.5 Hz linewidth with Lorentzian lineshape on $CHCl_3$.[10, 34]

Increasingly, solids probes are being used for biological applications at high fields,[1, 6, 9] and in these applications it is extremely important to minimize rf sample heating during high power decoupling.[7, 14, 35] To this end, it is critical to minimize E/B_1, as relative dielectric heating is proportional to the square of this ratio.[7] The conservative electric field (the part that does not come from $d\boldsymbol{B_1}/dt$) in a solenoid is often more than three times the minimum achievable E field at a given B_1. The E/B_1 ratio is reduced by a factor of 2-3 in the "scroll coil", but its extra low inductance (as needed to limit the self resonance) leads to lower S/N in multi-tuned coils.[35]

The "cross coil" [7, 32] (XC), a numerically optimized derivative of the Alderman-Grant and Litz coils,[36, 37] appears to offer about another factor-of-two drop (compared to the scroll coil) in dielectric heating for the 4 mm case.[7] In this approach, the XC is used for ^{1}H only, and an outer solenoid is double tuned for the mid-frequency (MF) and low-frequency (LF) channels. A related, inverted approach (with the solenoid as the inner coil and the saddle coil as the outer coil) has also been demonstrated in a PISEMA application.[14] Both approaches eliminate the problem of achieving high B_1 homogeneity from a solenoid above its self resonance,[38, 39] but the latter approach may not be compatible with MAS at high fields.

Both experiments and simulations show that the best resolution that can normally be obtained in a conventional wide line (non-spinning, or "static") probe using a heavy copper solenoid (with typical attention to filling factor, and shimmed for reasonable lineshape) is ~0.2 ppm, with about 2 ppm line width at 2% of peak height. As linewidths in proteins in bicelles in solutions are ~20 Hz (0.025 ppm at 800 MHz), there is reason to believe that PISEMA experiments could benefit from high-power solids probes designed for high spectral resolution. The usual solution to the resolution problem in microcoils is to immerse the copper coil in a non-protonated fluid (such as 3M FC-43) of susceptibility similar to that of copper. Linewidths under 0.01 ppm have thus been achieved with sample diameter 80% of the coil i.d.,[28] though lineshape is usually not very close to Lorentzian. However, liquid-emersion compensation methods may not be practical with large-sample, low-E, high-power probes.

Many early analytical methods for calculation of the magnetic field profile had limited accuracy, as they often assumed uniform current distributions across the conductors, or current distributions based on crude approximations; and calculations of $\boldsymbol{E}$ fields within the sample were seldom attempted until recently. Accurate full-wave numerical methods for calculating the fields have been available in commercial software (Ansoft HFSS, CST MWS, REMCOM, Vector Fields, etc.) for the past decade, and recently at least two of these packages have been shown to calculate all the relevant losses (conductor surface currents, sample dielectric, radiation, lumped elements) with remarkable accuracy – often within 5%.[7, 40]

Table 2 lists various materials properties, some measured in our laboratory and some collected from various sources,[18, 31, 41-45] for materials commonly found in NMR probes. The magnetic susceptibility data are at 7 T, though field dependence is usually small. The dielectric loss data are for 500 MHz and 450 K, but the rest of the data are for room temperature. Note that in some cases there are large differences between the listed loss data and the more commonly published values for 300 K, 1 MHz.

Table 2 Properties of NMR Probe Materials

(a) **Conductors**

Material	Density	Young's modulus	Solidus Temp.	Yield strength	Electrical conductivity	Thermal conductivity	Thermal expansion	Specific heat	Magnetic susceptibility
Symbol	d	E	T_M	S	σ	k_T	b_T	C_p	χ_v
Units	kg/m^3	GPa	^{0}C	MPa	M(Ωm)$^{-1}$	W/m-K	10^{-6}/K	J/kgK	10^{-6}
Aluminum	2700	69	660	30	36.6	230	22	900	20.7
Copper	8950	122	1083	150	58.0	400	16.5	490	-9.66
Gold	19300	78	1064	20	44.0	315	14.2	128	-34.6
Hafnium	13090	110	2227	300	2.9	22	5.9	145	65
Iridium	22500	440	2410	1200	19.8	147	6.8	130	37
Molybdenum	10200	320	2617	300	18.1	138	5.2	276	96
Palladium	12020	115	1552	250	9.3	76	11.8	245	~1000
Rhodium	12440	330	1966	800	20.9	150	8.3	247	155
Silver	10500	78	962	100	61.4	428	19	235	-23.8
Tungsten	19250	410	3410	1000	18.4	173	3.8	133	69
Zirconium[a]	6506	99	1852	200	2.3	21	5.85	295	160
Al-6061T6[b]	2700	69	582	214	25	180	23.6	896	20
CuNiAlCr[c]	8900	150	1150	400	2.3	26	16	380	60
H. C-22[d]	8690	206	1357	400	0.9	10	12.4	414	590
SiNi-Bronze[e]	8780	115	960	550	23.5	36	17.5	380	0.6
Sn-Bronze[f]	8860	110	975	200	11.5	84	17.8	380	-10
63/37PbSn	9700	30	183	40	6.3	45	22	176	-3.5
96/3.7SnAg	7500	30	221	55	8.3	70	20	220	0.7
SS304[g]	8000	193	1400	300	1.4	16	17	500	3000

(b) Insulators

Material	Density	Young's modulus	Yield Strength	Dielectric constant	HT Loss tangent	Thermal conductivity	Thermal expansion	Specific heat	Magnetic susceptibility
Symbol	d	E	S	k_d	ε''	k_T	b_T	C_p	χ_v
Units	kg/m^3	GPa	MPa			W/m-K	10^{-6}/K	J/kgK	10^{-6}
99.5Al_2O_3	3950	390	240	9.9	0.0001	35	8	780	-14
Epoxy[h]	1200	2.3	60	3.6	0.02	0.34	54	1400	-11.5
Kel-f	2100	1.3	20	2.5	0.02[i]	0.21	60	800	-11.6
Macor[j]	2520	64	80	5.7	0.007	1.7	9	750	-11.7
99.5MgO	3400	250	100	9.6	0.0001	20	13.5	955	-17.8
PEEK	1300	3.8	70	3.3	0.003	0.24	54	1500	-9.3
Pyrex-7070	2500	70	60	4.0	0.002[s]	1.3	3.3	800	-11
Quartz[k]	2250	74	50	3.8	0.0001	1.4	0.5	700	-11.8
Radel PPS	1350	2.7	60	3.0	0.007	0.35	50	1200	-9.2
Silica Foam[l]	770	~20	~5	~1.5	0.0001	~0.1	0.5	700	-3.5
Silicone[m]	1080	0.5	7	2.8	0.008	0.3	~30	1800	-7.5
Si_3N_4[n]	3250	310	800	9	0.002[s]	27	3.2	740	-14
Teflon	2200	0.4	12	2.1	0.0003	0.25	120	750	-10.5
Torlon5030[o]	1610	11	205	4.2	0.01[s]	0.37	16	950	~-6
Ultem PEI	1270	2.7	90	3.2	0.0025	0.3	55	1300	-9.0
Vespel SP1[p]	1430	3.1	86	3.5	0.005	0.33	54	1130	-9.2
V-TP8169[q]	1320	3.2	90	3.1	0.0014[s]	0.18	54	1100	-9
Water	997	0	0	75	-	0.6	-	4182	-9.06
Zirconia[r]	6050	210	700	29	0.02[s]	2.2	10	400	-8.8

Notes: Volume susceptibility χ_v in SI is related to cgs molar susceptibility χ_m by: $\chi_v = 4\pi d\chi_m / (M.wt.)$.

a. Grade 702: 96Zr, 3Hf, 0.1Cr, 0.1Fe.

b. 97Al, 1Mg, 0.6Si, 0.3Fe.
c. Custom: 73Cu, 20Ni, 3Al, 2.5Cr, 0.5Mo, 0.01Fe.
d. Haynes C-22: 60Ni, 22Cr, 13Mo, 5W + Co.
e. Custom: 92Cu, 3Si, 2.4Ni, 1.8Sn, 0.4Pb, 0.07Fe.
f. C51000: 95Cu, 5Sn, 0.2P, 0.05Fe.
g. 68Fe, 19Cr, 9Ni, 2Mn, 1Si.
h. Epo-Tek 353ND
i. ε''=0.003 at 300 K
j. Al-B-Si-Mg-F ceramic glass, Corning.
k. Fused silica, electronic grade.
l. Fused silica foam, industrial grade.
m. Clear RTV
n. Kyocera SN240
o. PAI resin, 30% glass fiber.
p. Dupont polyimide SP-1.
q. Vespel TP-8169, similar to Aurum-450.
r. CoorsTek YTZP, 92ZrO_2, 3HfO_2, 5Y_2O_3.
s. Estimate, based on data for a similar material.

4 WIDE LINE

The initial instrumentation for solids NMR borrowed extensively from radar and UHF transmitter technology, using fixed-frequency transmission lines as circulators and magic-Ts to isolate the multi-kilowatt transmitter from the low-noise preamplifier.[46] It was soon determined that it was not usually difficult to deal with the phase transients from Q_L of 40-150. (Note: See discussion of the different Q definitions in ***Probe Design and Construction***. A very recent trend is to report (matched) Q_L, which is half the common definition of Q in earlier NMR and EPR literature.) Hence, several hundred watts were sufficient except perhaps for low-γ nuclei. The cost savings of moderate power transmitters and the shift from transmission line traps to lumped elements facilitated the commercial solids probe,[47] which is often required to be multinuclear and reasonably user-friendly.

A number of accelerated ringdown schemes have been proposed, but the method seeing more use today is overcoupling [48, 49] because of noise and reliability problems associated with active switching methods. Moreover, the recent availability of linear prediction often obviates the need for active damping (see ***Fourier Transform and Linear Prediction Methods***). However, it is still sometimes beneficial to dampen Q_L to ~40, and one method is coating the coil with tin-lead solder.

The unbalanced, capacitively matched DT circuit (see ***Probe Design and Construction***, Figure 6) is often used for wideline probes to simplify multinuclear tuning. The HF tuning coil L_H (which may be a capacitively shortened $\lambda/4$ coaxial transmission line) is normally chosen to have an inductance such that its untuned reactance would be between 25 and 60 Ω at the HF. Lead inductance is minimized subject to VT, high voltage, and multinuclear constraints. The total series lead inductance is then typically 20-40 nH.[21] Maximum B_1/V_T, where V_T is the maximum total circuit voltage, is obtained for sample coil inductance L_S half of the total circuit inductance, but a somewhat higher value is usually selected for improved LF sensitivity with some sacrifice in HF efficiency and a slight reduction in maximum B_1.

A number of researchers have found it easier to achieve high efficiencies in high-power probes using transmission lines in place of some of the lumped elements, especially at lower and moderate fields,[50, 51] and some have extended such circuits to triple resonance at high fields.[6] However, such circuits have not been shown to be compatible with multi-nuclear tuning at high fields and have disadvantages with respect to phase transients compared to circuits not using very-high-Q resonators.[7]

As previously mentioned, the applications are increasingly with biological samples where it is necessary to reduce decoupler heating. For example, in a 4 mm MAS probe based on a triple-tuned solenoid at 750 MHz with a biological sample, most of the ^{1}H power will be dissipated in the sample, and the

mean sample temperature increase will be 30-60^{0}C per watt of average rf power, depending mostly on the rotor cooling method.[7] High-field triple-resonance wide-line probes are increasingly using an inner ^{1}H XC and an outer solenoid, double-tuned for the MF and LF, similar to the MAS case.[7, 10, 13, 32]

Minimum 90^0 pulse lengths have usually been 2-3 μs, but Hadamard NMR offers a low-power alternative.[52, 53] In Hadamard NMR, the spin system response to the application of a large number of pseudorandom pulses with flip angles as small as 0.1^0 (mW, μs pulses) at periods on the order of tens of microseconds can be transformed into the equivalent NMR response of a single high-power pulse. SNR for Hadamard appears comparable to Fourier Transform (FT) under certain conditions. (See also ***Stochastic Excitation***.)

5 MAGIC ANGLE SPINNING

In 1958, Raymond Andrew showed that high-speed sample spinning at the 'magic' angle of 54.7^0 could be an effective tool in averaging out dipolar broadening.[54] However, the required rotational rates for abundant dipolar nuclei (>35 kHz for ^{1}H) appeared impossible, and the technique was largely ignored[46] for nearly two decades until Stejskal and Schaefer [5] showed that more realistic rotational rates (2 to 5 kHz), capable of averaging chemical shift anisotropy and susceptibility broadening, combined with high-power decoupling to remove the ^{1}H dipolar broadening, could be extremely effective in obtaining high-resolution ^{13}C spectra from solid samples.

Andrew used a conical bearing/drive surface which eventually achieved speeds in excess of 10 kHz using helium gas.[55] This spinner was based on the classic ultracentrifuge work by Beams[56] and depended on the Bernoulli effect to hold the sample spinner close to the drive jets. The stiffness of such a bearing is extremely low, which results in low-frequency oscillations, precession, and instabilities. Moreover, angular accuracy of 0.3^0 is sometimes required in MAS, which is an order of magnitude beyond the capability of the conical Bernoulli-Beams bearing. Lippmaa, Veeman, Pines, Eckman, and others introduced the double-bearing cylindrical rotor to circumvent these problems,[57] and Doty and Ellis presented an approximate analysis of the cylindrical air-bearing optimization.[58] [Note that typographical errors resulted in equations (9) and (12) in the referenced article appearing twice.[58] The second equation in each case is correct. The first should be deleted.]

5.1 Rotor and Cap Materials

High-strength ceramics, where much progress has been made over the past decade,[18, 19] are required to obtain high sensitivity (from high filling factor) and high spinning speeds simultaneously.[57] Partially stabilized zirconia (PSZ) has usually been used in MAS probes for rotors and stators because of its outstanding mechanical and magnetic properties. Silicon nitride, Si_3N_4, has been the promising "material of the future" for three decades,[58] as it has the highest demonstrated strength-to-mass ratio of any available ceramic and this allows the highest surface speeds. However, the technical difficulties in producing it with low defects have given it a checkered history. A quartz-glass-encapsulated, hot-isostatic-pressing process was successful in producing parts of acceptable quality for MAS rotors,[59] but it was discontinued for economic reasons. Recently, a new sintering process has been developed by Kyocera that seems to be consistently producing a high grade material (Kyocera SN240, composition not yet reported) with very low defects, high fracture toughness, high tensile strength, low dielectric loss, very low magnetism, and acceptable cost in small batches.[60] (The silicon nitride grades that are now commonly used in the ball bearing and automotive exhaust-valve applications are too magnetic for most NMR applications, as the "Ford-type" sintering processes require a significant iron oxide component – typically ~1400 ppm Fe.) Even though material defects should no longer continue to be a problem in production of silicon nitride rotors, they will always be much more expensive than zirconia, as the diamond tooling wear rates and time required for internal grinding and honing are greater than for zirconia by at least a factor of five.

The press-fit turbine caps are usually machined from a high-strength plastic or composite, several

of which are listed in Table 2b. Zirconia, silicon nitride, and macor have also been used for high-temperature applications. Achieving the required tolerances on these components is very demanding.

5.2 High-Speed Air Bearings

The high mass of ceramic rotors requires more attention to rotor resonances than was required in the earlier designs using plastic rotors.[61] For stability throughout a wide speed range, it is advantageous to have the high bearing stiffness that comes from relatively tight radial clearances. However, as the clearance is reduced, bearing frictional heating becomes more severe; moreover, the possibility of a 'crash' increases. A crash may occur in a hydrostatic bearing when the rotor moves close enough to the stator to cause extreme choking around the perimeter of the bearing nozzles on the proximal side, at which point the stiffness changes sign and the rotor is driven into the stator. Pockets or recesses at the orifice exit may eliminate this crash mechanism,[58, 62] but the reduced response time adversely affects stability at very high speeds unless the pockets are very small.[63]

Highest surface speeds have probably been obtained with the 5 mm "supersonic" design shown in Figure 2 and several similar designs (XC4 and XC5),[32, 64] which have achieved surface speeds in excess of the speed of sound at room temperature. (For example, 4 mm rotors now routinely spin above 27 kHz). Half of the bearing gas exits over the ends of the rotor forming an axial thrust bearing at each end, while half exits out the center of the stator. Allowing the gas to flow axially inward as well as outward increases the bearing stiffness (by nearly doubling effective area), and this was probably the most significant innovation in the spinner by Langer et al., which achieved a 40% increase in surface speed over previous designs.[65] Extremely high surface speeds have rather recently been achieved in rotors as small as 1.3 mm diameter with rotational rates up to 70 kHz.[12, 66]

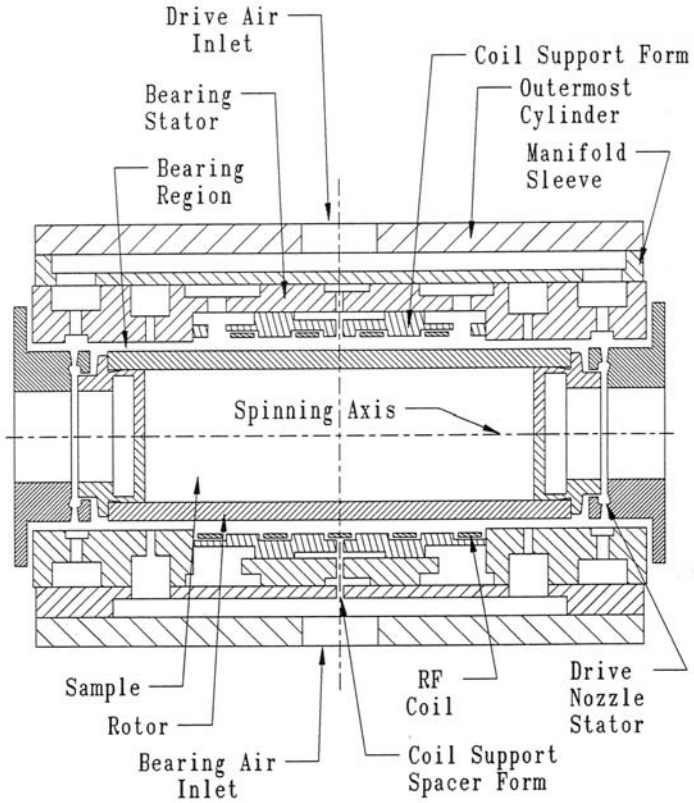

Figure 2 Supersonic sample spinner (Doty Scientific, Inc.)

Optimum bearing radial clearance for controlling Taylor vortices in the air bearing at moderate speeds is roughly proportional to $(\mu^2 d/c^2\rho^2)^{1/3}$ where μ is the gas viscosity, d is the rotor diameter, c is the velocity of sound, and ρ is the gas density.[58] Optimum clearance r_c for the control of whirl instabilities with minimum friction at high speeds fits the following empirical equation for typical NMR spinners:

$$r_c \cong kT^{0.25}d^{0.4} \qquad \text{(mixed units)} \qquad (2)$$

where T is the gas temperature (K), d is the rotor diameter in mm, and k has an approximate numerical value of 0.0027 for nitrogen and 0.0035 for helium with units $K^{-0.25}\,mm^{0.6}$. It is necessary to take into account the strain that will occur even in ceramic rotors at top speeds: 0.1% and 0.15% for silicon nitride and zirconia, respectively. Optimum bearing hole size is such that bearing mass flow at 0.3 MPa with the rotor in place is 60%-85% of the mass flow with the rotor removed. Short bearing hole sizes normally range from 0.12 mm for 3.5-mm rotors to 0.28 mm for 14-mm rotors.

5.3 High-speed Spinner Turbines and Axial Stabilization

For surface speeds above 250 m/s (without helium drive gas), it can be beneficial to use microturbines in a symmetrical fashion so that axial reaction forces are precisely balanced at all speeds, since the load capacity of the axial thrust bearings is quite limited.[67] The reduced-diameter radial-inflow microturbines used in Figure 2 achieve much higher isentropic efficiency than the earlier Peltier microturbines by (a) controlling flow separation over the blades, (b) operating at lower tip speed, and (c) reducing exhaust swirl.[68] A vaneless radial-inflow supersonic diffuser may be used with the larger sizes to obtain supersonic, non-separated flow at the rotor entrance. The microturbines on a 14-mm rotor have 28 blades with 10-mm tip o.d. and produce 25 W shaft power each at 40% isentropic efficiency at 6 kHz. The 3-mm o.d. microturbines on a 4-mm rotor have only 11 blades and achieve 15-20% efficiency at 20 kHz, depending on various details. Unlike large turbines, substantial efficiency losses occur in the nozzles (even with the 14-mm spinners) because of boundary layer effects.

A major drawback of spinner designs with shrouded drive turbines at both ends, as that of Figure 2, is that they are not compatible with auto sample eject. It is also more difficult to load rotors manually in designs of this type. As a result, the "drop-in" spinner designs have been more popular. Substantial progress has been made recently in improving both their spinning speed[12, 66] and their axial stability.[10, 13]

Many of the drop-in designs have been somewhat similar to the Beams design[56] with the improvements of Bartuska et al.[61] In this approach, an outflow Bernoulli bearing is formed between the conical tip on the lower end of a rotor (of included angle ~100^0) and the conical stator-bearing surface (of included angle ~90^0). A number of gas-feed holes through this conical stator surface at compound angles produce rotational outward gas flow in the clearance space. Owing to the converging nature of this conical flow space, the radial component of the flow velocity may be sufficiently high at the periphery for a substantial Bernoulli effect, which, depending on various conditions, may exceed the hydrostatic effects nearer the center. As a result, a reasonably stable axial bearing may be formed over a rather wide range of spinning speeds, assuming sufficient space is available near the periphery of the conical surfaces for the gas to exhaust with very low back pressure.

Recently, unsuccessful attempts to apply a drop-in spinner similar to that described above to a cryogenic MAS probe with auto-sample eject stimulated the development of an inflow Bernoulli bearing.[11] It was shown that it appears to be theoretically impossible to achieve significant rotational drive and good axial stability in a conical inflow bearing, but axial stability much better than normally achieved in the Bartuska-type drive can be achieved if an inflow bearing is designed only for optimum axial stability and the rotational drive requirement is met using a radial inflow turbine at the other end.

5.4 Radiofrequency Circuits

Most of the circuits that have been used in wideline solids probes, some of which were mentioned

earlier, have also been used in MAS.[6, 7, 47, 50, 51, 69, 70] The primary difference is that rf power levels are usually lower in MAS because the sample is smaller, but this does not imply that voltage breakdown is not an issue, as the spinner assembly imposes severe dimensional constraints. Another difference is that lead inductance is usually more significant in MAS, especially if spinner reorientation for sample eject is implemented.

Single-resonance circuits are sufficient for some purposes, such as ^{1}H CRAMPS (combined rotation and multiple-pulse spectroscopy). In such cases, very low inductance coils (perhaps only 2 turns) are well suited, though it is more difficult to achieve high $\boldsymbol{B}_1$ homogeneity with a small number of turns – except with the scroll coil, which has distinct advantages in this respect.[7, 35]

For efficient CP at high speeds, high rf homogeneity is much more important than originally recognized, even though variable amplitude proton $\boldsymbol{B}_2$ can greatly improve CP efficiency in the presence of large rf inhomogeneity.[71] At high fields, even with small samples, it becomes quite important to balance the HF channel for more predictable $\boldsymbol{B}_2$ profile. Sufficiently accurate field matching at the different resonances is otherwise difficult to achieve.[70] In single-coil circuits, this is usually done using a small lumped-element trap (which often accounts for a substantial portion of the ^{1}H losses), even when transmission lines are used for much of the rest of the circuitry.[6] In multi-coil circuits, a dedicated ^{1}H orthogonal coil may be more simply capacitively balanced.[7, 14, 32]

Beginning with the development of the rotational echo double resonance (REDOR) technique for accurate distance determinations from weak dipolar couplings,[72] a large number of techniques have been developed that require triple-resonance MAS probes. The circuit shown in Figure 3, or one quite similar, has been used frequently for the LF and MF channels in triple-resonance probes in which the ^{1}H is handled by an inner, segmented saddle coil, while an external solenoid handles the multi-nuclear LF and MF. (Note that arbitrary node identification numbers, as required by circuit simulation software, are included.) This approach has been proven advantageous at ^{1}H frequencies up to 930 MHz in narrow-bore magnets,[73] primarily because of the order-of-magnitude reduction in rf sample heating from the segmented ^{1}H cross coil, but also because the two-coil approach is much more compatible with the long leads needed for auto sample eject.[10] It has also demonstrated superior S/N on samples requiring very high decoupling power, even when sample conductivity is low.[7]

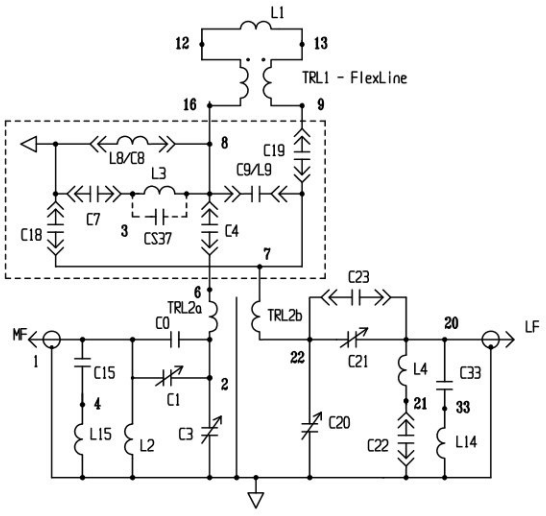

Figure 3 Doubly broadband, LF/MF circuit for the outer solenoid in a triple-resonance probe

A common characteristic of high-field, multi-nuclear triple-resonant circuits is that rf efficiencies are not particularly impressive – often in the range of 20-40%.[6, 7] Hence, there is an opportunity for significant improvement in S/N from cryogenic cooling of the tuning elements external to the sample coil. A S/N gain of 55% on the MF channel was recently reported from cooling of the critical tuning elements to

90 K while the sample remained at RT.[10] A drawing of this probe, with the cold zone below the spinner zone, is shown in Figure 4. Achieving this S/N gain also requires a preamp with an ultra-low noise figure (~0.6 dB), as the improvement comes more from the reduction in mean noise temperature than from increased Q.

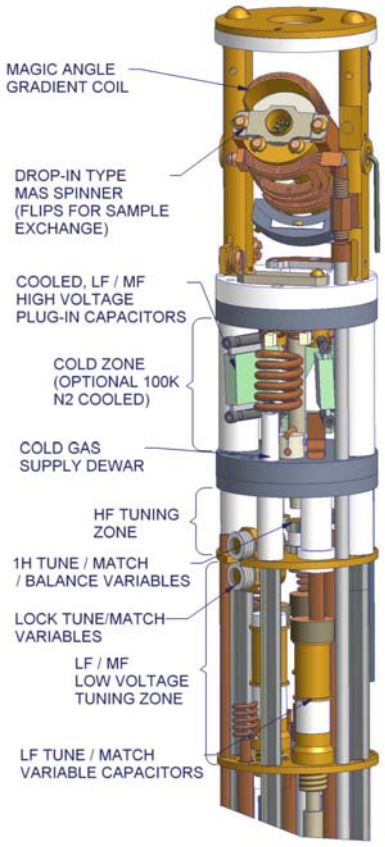

Figure 4 Drawing of a triple-resonance MAS probe compatible with cryogenic S/N enhancement

Gradient-enhanced spectroscopy has become a standard and powerful tool in NMR of liquids, especially for coherence selection, water suppression, and diffusion measurement. While a single z-gradient is often adequate, applying the gradient at the magic angle can be beneficial, especially in MAS, as it eliminates the modulation that otherwise results from off-axis gradients, which can present difficulties in assignments.[74, 75] Two designs for Magic Angle Gradient (MAG) coils have been published,[76, 77] and a numerical hybridization of these appeared shortly thereafter, optimized for high gradients (up to 250 G/cm) and minimum torques (to minimize vibration).[78]

6 VARIABLE TEMPERATURE (VT)

Many CP MAS probes operate from -120 to +160^{0}C, but XVT CP MAS probes are available for wider temperature ranges. The standard approach is to control the temperature of a gas stream (using a heater and thermocouple) that flows over the surface of the rotor.

One confounding factor in MAS thermometry is that frictional heating from MAS is proportional to the square of the surface speed,[58] and peak heating within the air bearing typically exceeds 80^{0}C for surface speeds about 90% of the speed of sound. The MAS design of Bartuska et al [79] provides clear separation between the VT and the bearing gas, which significantly reduces the frictional heating of the

sample compared to several alternative designs. At this point, it seems all recent commercial spinner designs have addressed this issue adequately, though it was a serious problem in some of the earlier designs.

The other (and often more serious) complication is the effect of rf heating, as very high rf magnetic field strengths are often required. As noted earlier, with a 4 mm rotor, the mean sample temperature increase will be 30-60^{0}C per watt of average rf power deposited in the sample. One way of dealing with this issue is to reduce the rotor size, as the peak temperature rise from rf heating is approximately proportional to the fourth power of the rotor radius for a given mean decoupling field strength.[7] The other approach is to use novel coil designs with reduced ratio of $\boldsymbol{E}/\boldsymbol{B}_1$.[7, 14, 35]

The enormous success over the past decade of cryoprobes for liquid samples,[80, 81] in which the sample may be near room temperature while the critical electronic components are cooled to ~25 K, has stimulated interest recently in cryogenic probes for solid samples.[11, 82, 83] MAS has been demonstrated on research apparatus at temperatures at least down to 16 K,[82] and wideline CP experiments have been carried out at temperatures down to 2 K.[84] At the other end of the temperature extreme, CP MAS probes are commercially available for sample temperature up to 750^{0}C.[34]

7 SPECIALIZED SOLIDS NMR PROBES

Quite a number of very specialized solids probes have been developed over the years for specialized solids applications of MAS and wideline methods (extremely low or high temperatures, or very small or large samples, or unique combinations of frequencies), but in this section we look briefly at several radically different approaches to obtaining high spectral resolution in solids. Three characteristics the clever techniques reviewed here have in common are (1) they require highly specialized hardware, (2) they are not currently in wide-spread usage, and (3) suitable probes have been made commercially.

7.1 Goniometers and Slow MAS

The earliest applications of NMR to solids involved the study of single crystals, where relatively narrow lines are observed without multiple pulse or high-speed spinning techniques. These studies are necessarily limited to materials that can be obtained in single crystals of sufficient size (usually several mm^3) for acceptable S/N. The method requires the ability to slowly and precisely rotate the crystal about three orthogonal axes while observing the anisotropic chemical shift. The common method for the past two decades has involved gluing a small crystal into a three-sided, 4-mm 'semi-cube'.[8] The sample may then be inserted into a precision holder inside the sample coil for 360^0 rotation about an axis perpendicular to $\boldsymbol{B}_0$ in small increments at which spectra are collected. The semicube is then removed and reinserted for rotation about a second axis, and the process is repeated again for the third axis. The crystal orientation with respect to the semi-cube holder is determined using X-ray crystallographic techniques.

The sample holder axis may be inclined at the magic angle to permit slow MAS, which is a method of addressing the spinning sideband problem by applying pulses precisely at 0^0, 120^0, and 240^0. There is renewed interest in this technique for obtaining high-resolution localized spectra from live mice.[85] (Also, see ***Magic Angle Turning and Hopping***.) Rotation has been accomplished by a variety of methods, including aluminum or brass bevel gears, worm gears, belts, flexible shafts, manual goniometers, and stepper motors under computer control.

7.2 DOR and MQMAS

In the Double Rotation (DOR) technique for quadrupolar nuclides, the sample is placed in a small spinner inside a larger spinner and spun about two intersecting axes simultaneously to accomplish the time averaging needed to remove both dipolar and quadrupolar interactions.[86, 87] It usually comes as a surprise to the uninitiated that such a feat would be possible at high speeds, even though most have observed a football traveling through the air executing free precession – spinning about two axes simultane-

ously with no significant external torques acting upon it. The requirement for no net torques on the inner rotor is given by the following:

$$f_1 = \frac{f_2 (I_T - I_A) \cos \theta_2}{I_A} \tag{3}$$

where f_1 is the frequency of the inner rotor, f_2 is the frequency of the outer rotor, I_A is the axial moment of inertia of the inner spinner (rotor, sample, caps), I_T is the transverse moment of inertia of the inner spinner, and θ_2 is the angle of the inner rotor with respect to the axis of the outer rotor.[87]

In practice, the outer rotor is always inclined at the dipolar magic angle, 54.7^0, and θ_2 is 30.56^0. For stability, (a) f_1 must be a few percent larger than given by the above, (b) the center of mass of the inner rotor must lie precisely on the axis of the outer rotor, and (c) the outer rotor must be dynamically balanced when the inner rotor is removed. Rotational rates up to 1800 Hz for the outer and 18 kHz for the inner rotor have been achieved within the constraints of a narrow-bore, 600 MHz magnet.[88] However, the technical difficulties have been such that this technique has largely been supplanted by multiple quantum MAS (MQMAS) and other methods for quadrupolar nuclides.[89] MQMAS probes are still demanding, as they require very high rf field strengths, but these technical challenges are much more manageable, especially with small samples.

7.3 SAS and STMAS

High-resolution NMR spectra can be obtained from quadrupolar nuclei if the sample spinning axis can be rapidly reoriented such that the time average of the second and fourth spherical harmonic functions vanishes.[86, 90] Similar hardware is also useful in the determination of residual dipolar couplings in bicelles. When a sample containing discoidal bicelles of negative magnetic anisotropy is spun at the magic angle, their interactions with $\boldsymbol{B}_0$ vanish and their orientations becomes random. For sample spinning at angles less than 54.7^0, they align with their normals perpendicular to the spinning axis, while spinning at greater angles causes their normals to align with the spinning axis.[91] Dynamic control over the spinning axis can provide protein alignment control that is useful in more effective utilization of the bond angle information inherent in the residual dipolar coupling.[92]

The switched angle spinning (SAS) or dynamic angle spinning (DAS) probe allows the spinning axis to be rapidly changed while spinning the sample at high speeds to accomplish the desired averaging or director control. One early design used a pneumatic system to switch between two fixed angles, but a high-performance servo motor and precision encoder are now generally used, as programming flexibility is often needed.[13]

Two basic approaches have been used: moving coil, and fixed coil. The fixed coil design used a small spinner assembly that could be rotated perpendicular to its spinning axis inside a large rf coil that was perpendicular to the external field and coaxial with the reorientation axis. The moving coil design has the rf coil (or coils) mounted on the spinner stator and attached with flexible leads or sliding contacts, and it has proven more satisfactory.[93]

A simplified analysis suggests high-torque, low-inertia servo motors with optimized linkage might permit axis reorientation in under 12 ms. However, linkage compliance, structure vibrations, control limitations, and air bearing stiffness typically limit switching times to ~22 ms, and an additional 5-15 ms is required when very accurate settling is needed. Spinning rates above 10 kHz have been achieved using a drop-in 4 mm spinner during rapid angle switching.

One of the factors contributing to the engineering difficulties is that the servo motor must be positioned well below the magnet to operate properly, which requires a rather long drive linkage that still must allow easy insertion of the probe into the magnet. Another challenge has been getting the leads to survive hundreds of thousands or even millions of flips. This has favored the use of sliding contacts, at least for the LF and MF channels. A photo of a recent SAS probe is shown in Figure 5.

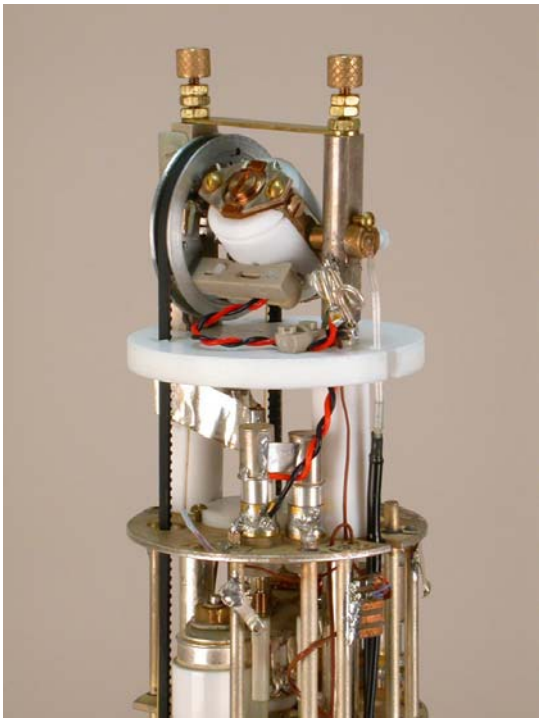

Figure 5 Photo of a WB SAS probe using an XC4 spinner. A fused glass-fiber light pipe is visible coming in along the reorientation axis on the near side for optical spin-rate detection. The MF/LF lead connections on the opposite side are not visible in this view, but are handled in a way similar to commutator connections in some DC motors.

Several methods for quadrupolar nuclides benefit from magic angle setting repeatability of less than 0.01^0,[94] and a particularly demanding method in this respect is satellite transition MAS (STMAS).[95] The STMAS experiment offers an alternative approach to earlier methods such as DAS, DOR, and MQMAS for obtaining high-resolution NMR spectra of half-integer quadrupolar nuclei. Unlike the multiple-quantum experiment, STMAS involves two-dimensional correlation of purely single-quantum coherences. The technique requires high stability in spinning rate control as well as extremely high accuracy in angle setting. Probes with auto sample exchange have generally been found to have better angle repeatability than conventional MAS probes without this capability.[95] Angle repeatability of better than 0.02^0 has recently been demonstrated in a multinuclear triple-resonance 4 mm VT SAS probe that included a PFG coil and optical spinning rate detection.[13]

8 RELATED ARTCLES

Probe Design & Construction; Magic Angle Spinning; Extended Magic Angle Spinning; Double Rotation; Dynamic Angle Spinning; Satellite Transition NMR Spectroscopy of Half-Integer Quadrupolar Nuclei under Magic-Angle Spinning; Advances in MQMAS NMR.

9 REFERENCES

1. M. J. Duer, “Introduction to Solid State NMR Spectroscopy”, Blackwell Pub., Oxford, 2004.
2. M . H. Levitt, “Spin Dynamics”, Wiley, 2001.
3 S. R. Hartmann and E. L. Hahn, "Nuclear Double Resonance in the Rotating Frame," *Phys. Rev.*, 1962, **128**, 2042-53.

4. R. W. Vaughan, “High Resolution Solid-state NMR”, *Annu. Rev. Phys. Chem.*, 1978, **29**, 397-419.
5. E. O. Stejskal, J. Schaefer, and J. S. Waugh, "Magic-Angle Spinning and Polarization Transfer in Proton-Enhanced NMR," *J. Magn. Reson.*, 1977, **28**, 105-112.
6. R. W. Martin, E. K. Paulson, and K. W. Zilm, “Design of a triple resonance MAS probe for high field solid-state NMR”, *Rev. Sci. Instrum.*, 2003, **74**, 3045-3061.
7. F. D. Doty, J. Kulkarni, C. Turner, G. Entzminger, A. Bielecki, “Using a cross-coil to reduce RF heating by an order of magnitude in triple-resonance multinuclear MAS at high fields”, *J. Magn. Reson.*, 2006, **182**, 239-253.
8. R. S. Honkonen, F. D. Doty, P. D. Ellis, "^{113}Cd Shielding Tensors of Cd-O Compounds: Single Crystal Studies of $Cd(NO_3)_2 4H_2O$," *J. Am. Chem. Soc.*, 1983, **105**, 4163.
9. F. M. Marassi and S. J. Opella, “Simultaneous assignment and structure determination of a membrane protein from NMR orientational restraints”, 2003, *Protein Science*, **12**, 403-411.
10. F. D. Doty, G..Entzminger, S. Shevgoor, D. Arcos, and J. P. Staab, “Improving S/N by 55% in a triple-resonance narrow-bore MAS probe with minimal RF sample heating”, Pres. at SEMRC, Gainesville, FL, 2006.
11. F. D. Doty, S. Shevgoor, J. B. Spitzmesser, “Progress on 4-channel 3 mm CryoMAS Probe with Auto Sample Exchange for High-field Solids NMR”, Presented at EuroMAR, York, UK, 2006.
12. A. R. Palmer, M. Cormos, C. E. Bronnimann, S. Hafner, “Solid State ^{1}H Observe NMR Spectroscopy with 70 kHz MAS”, poster 288, presented at the 47th ENC, Asilomar, 2006.
13. G. Entzminger, V. Cothran, J. Staab, J. B. Spitzmesser, S. Shevgoor, L. Li, J. R. Doty, J. Kulkarni, L. L. Holte, and F. D. Doty, “Development of a Triple-resonance SAS Probe with Field Gradient Coil for Dynamic Control over Alignment of Proteins in Bicelles”, poster 213, presented at the 47th ENC, Asilomar, 2006.
14. P. L. Gorkov, E. Y. Chekmenev, M. Cotton, G. Veglia, J. J. Buffy, N. Traaseth, T. A. Cross, W. W. Brey, “Applications of Low-E Static Probes to High Frequency Membrane Protein NMR”, poster 454, presented at the 47th ENC, Asilomar, 2006.
15. P. Gorkov, E. Chekmenev, R. Fu, J. Hu, T. Cross, M. Cotton, W. W. Brey, “A large volume flat coil probe for oriented membrane proteins”, *J Mag. Reson.*, 2006, **181**, 9-20.
16. J. J. O’Dwyer, ‘The Theory of Electrical Conduction and Breakdown in Solids Dielectrics’, Oxford University Press (Clarendon), London/New York, 1973.
17. E. Nasser, "Fundamentals of Gaseous Ionization and Plasma Electronics," Wiley, NY, 1971.
18. C. A. Harper (ed.), ‘Handbook of Ceramics, Glasses, and Diamonds’, McGraw Hill, NY, 2001.
19. S. J. Schneider (ed.), 'Engineered Materials Handbook’, Vol. 4, ‘Ceramics and Glasses', ASM International, Novelty, OH, 1991.
20. R. C. Buchanan (ed.), ‘Ceramic Materials for Electronics’, Marcel Dekker, NY, 1991.
21. F. D. Doty, T. J. Connick, X. Z. Ni, and M. N. Clingan, "Noise in High Power, High Frequency Double Tuned Probes," *J. Magn. Reson.*, 1988, 77, 536-549.
22. E. A. Nenasheva and N. F. Kartenko, “Capacitor material based on bismuth niobate substituted with zinc”, US Pat 6 887 812, 2005.
23. S. L. Patt, "Method for Suppression of Acoustic Ringing in NMR Measurements," U.S. Pat. 4,438,400, 1984.
24. M. L. Buess and G. L. Petersen, “Acoustic ringing effects in pulsed NMR probes”, *Rev. Sci. Instrum.*, 1978, 49, 1151.
25. See, http://www.jenningstech.com/products/product.cfm , 2006.
26. F. D. Doty, "HV Capacitor Wand for Multinuclear NMR," US Pat. 4 710 719, 1987.
27. D. I. Hoult and R. E. Richards, “The Signal-to-Noise Ratio of the NMR Experiment”, *J. Magn. Reson.*, 1976, **24**, 71-85.
28. Y. Li, A. G. Webb, S. Saha, W. W. Brey, C Zachariah, and A. S. Edison, “Comparison of the performance of round and rectangular wire in small solenoids for high-field NMR”, *Magn. Reson. in Chem.*, 2006, **44**, 255-262.
29. P. A. Keifer, L. Baltusis, D. M. Rice, A. A. Tymiak, and J. N. Shoolery, "A Comparison of NMR Spectra Obtained for Solid-Phase-Synthesis Resins Using Conventional High-Resolution, MAS,

and HR-MAS Probes," *J. Magn. Reson. Ser. A*, **1996, 119**, 65-75.
30. T. M. Barbara, "Cylindrical Demagnetization Fields and Microprobe Design in High-Resolution NMR," *J. Magn. Reson. Ser. A*, 1994, **109**, 265-69.
31. F. D. Doty, G. Entzminger, Y. A. Yang, "Magnetism in NMR Probe Design Part I: General Methods," *Concepts in Magn. Reson.*, 1998, **10**(3), 133-156.
32. F. D. Doty, Y. A. Yang, and G. E. Entzminger, "Magnetism in NMR Probe Design Part II: HR MAS," 1998, **10**(4), 239-260.
33. D. I. Hoult, "The NMR Receiver: A description and Analysis of Design", *Prog. in Nucl. Magn. Reson. Spectrosc.*, 1978, 12, 41.
34. See, http://www.dotynmr.com/ , 2006.
35. J. A. Stringer, C. E. Bronnimann, C. G. Mullen, D. H. Zhou, S. A. Stellfox, Y. Li, E. H. Williams, C. M. Rienstra, "Reduction of RF-induced sample heating with a scroll coil resonator structure for solid-state NMR probes", *J. Magn. Reson.*, 2005, **173**, 40-48.
36. D. W. Alderman and D. M. Grant, "An Efficient Decoupler Coil Design which Reduces Heating in Conductive Samples in Superconducting Spectrometers," *J. Magn. Reson.*, 1979**, 36**, 447-51.
37. F. D. Doty, G. Entzminger Jr, and C. D. Hauck, "Error-Tolerant RF Litz Coils for NMR/ MRI", 1999, *J. Magn. Reson.*, **140**, 17-31.
38. C. Luchinat, M. Piccioli, R. Pierattelli, F. Engelke, T. Marquardesn, and R. Ruin, "Development of NMR Instrumentation to Achieve Excitation of Large Bandwidths in High-Resolution Spectra at High Field," *J. Magn. Reson.*, 2001, **150**, 161-166.
39. Frank Engelke, "Electromagnetic Wave Compression and Radio Frequency Homogeneity in NMR Solenoidal Coils: Computational Approach", *Concepts in MR*, **15**, 129-155, 2002.
40. W. W. Brey, A. S. Edison, R. E. Nast, J. R. Rocca, S. Saha, R. S. Withers, "Design construction and validation of a 1-mm triple-resonance high-temperature-superconducting probe for NMR", *J Magn Reson*, 2006, **179**, 290-293.
41. D. R. Lide (ed.), 'CRC Handbook of Chemistry and Physics', 86th edn., CRC Press, Boca Raton, FL, 2006.
42. J. R. Davis (ed.), 'Metals Handbook', 10th Edn., Vol. 2, ASM International, Materials Park, OH, 1990.
43. W. A. Woishnis 'Engineering Plastics and Composites', 2nd ed. ASM International, Materials Park, OH, 1993.
44. J. Baker-Jarvis et al, NIST Technical Note 1520, 'Dielectric and Conductor-Loss Characterization and Measurements on Electronic Packaging Materials', 2001.
45. B. Riddle, J. Baker-Jarvis, and J. Krupka, "Complex Permittivity Measurements of Common Plastics Over Variable Temperatures", *IEEE Trans. Microwave Theory & Tech.*, 2003, **51**, 727-733.
46. J. D. Ellett, M. G. Gibby, U. Haeberlen, L. M. Huber, M. Mehring, A. Pines, and J. S. Waugh, in 'Advances in Magnetic Resonance', ed. J. S. Waugh, Academic Press, New York, 1971, Vol. 5, pp. 117-176.
47. F. D. Doty, R. R. Inners, and P. D. Ellis, "A Multinuclear Double Tuned Probe for Applications with Solids or Liquids Utilizing Lumped Tuning Elements," *J. Magn. Reson.*,1981, **43**, 399-416.
48. G. C. Chingas, "Overcoupling NMR Probes to Improve Transient Response," *J. Magn. Reson.*, 1983, **54**, 153-7.
49. J.B. Miller, B.H. Suits, A.N. Garroway, and M.A. Hepp, "Interplay among Recovery Time, Signal, and Noise: Series- and Parallel-Tuned Circuits Are not always the Same", *Concepts in Magn. Reson.*, 2000, **12**(3), 125-136.
50. J. Stringer and G. Drobny ,"Methods for the analysis and design of a solid state nuclear magnetic resonance probe", *Rev. Sci. Instrum.*, 1998, **69**, 9, 3384-3391.
51. Q. W. Zhang, H. Zhang, K. V. Lakshmi, D. K. Lee, C. H. Bradley, and R. J. Wittebort, "Double and Triple Resonance Circuits for High-frequency Probes", *J. Magn. Reson.*, 1998, **132**, 167-171.
52. M. Greferath, B. Blumich, W. M. Griffith, and G. L. Hoatson, "Saturation in Deuteron Hadamard NMR Spectroscopy of Solids," *J. Magn. Reson.*, Ser. A, 1993, **102**, 73-80.
53. Jun Ashida, Eriks Kupce, Jean-Paul Amoureux, "Hadamard NMR spectroscopy in solids", *J.*

Magn. Reson., 2006, **178**, 129-135.
54. E. R. Andrew, A. Bradbury, and R. G. Eades, "NMR Spectra from a Crystal rotated at High Speed," *Nature* (London), 1958, **182**, 1659.
55. E. Andrew, L Farnell, M. Firth, T. Gladhill, and I. Roberts, "High-Speed Rotors for NMR Studies on Solids," *J. Magn. Reson.* 1969, **1**, 27.
56. J. W. Beams, "High Rotational Speeds," *J. Appl. Phys.*, 1937, **8**, 795-806.
57. E. T. Lippmaa, M. A. Alla, A. A. Salumyae, and T. A. Tukherm, "Sensor for Generating Nuclear Magnetic Signals," US Pat. 4 254 373, 1981.
58. F. D. Doty and P. D. Ellis, "Design of High Speed Cylindrical NMR Sample Spinners," *Rev. Sci. Instrum.*, 1981, **52**, 1868-1875.
59. J. Adlerborn, M. Burstrom, L. Hermansson, and H. T. Larker, "Development of High Temperature High Strength Silicon Nitride by Glass Encapsulated Hot Isostatic Pressing," *Mater. Design*, 1987, **8**, 229-232.
60. Kyocera materials data, http://global.kyocera.com/prdct/fc/product/pdf/material_e.pdf , 2005.
61. V. J. Bartuska and G. E. Maciel, "A Magic-Angle Spinning System for Bullet-Type Rotors in Electromagnets," *J. Magn. Reson*., *J. Magn. Reson.*, 1981, **42**, 312.
62. W. B. Rowe, 'Hydrostatic and Hybrid Bearing Design', Butterworths, London, 1983.
63. F. D. Doty, "High Speed Cylindrical NMR Sample Spinner," US Pat. 4 456 882, 1984.
64. F. D. Doty, L. G. Hacker, and J. B. Spitzmesser, "'Supersonic Sample Spinner," U. S. Pat # 5,508,615, 1996.
65. V. Langer, P. Daugaard, and H. J. Jakobsen, "Ultrahigh Spinning Rates for a 7-mm Rotor in Multinuclear CPMAS NMR Spectroscopy of Solids," *J. Magn. Reson.*, 1986, **70**, 472-475.
66. Ago Samoson, "Recent Advances in MAS," Presented at the Alpine Conf., Chamonix, 2003.
67. F. D. Doty, J. B. Spitzmesser, and D. G. Wilson, "High Temperature NMR Sample Spinner," US Pat. 5 202 633, 1993.
68. F. D. Doty, B. L. Miller, G. S. Hosford, D. G. Wilson, W. Huanbo, and J. D. Jones, "High Efficiency Microturbine Technology," '*Proc. IECEC-91*', 1991, Vol. 2, SAE, Warrendale, PA, p. 436-442.
69. F. D. Doty, 'Doubly Broadband Triple Resonance Circuit', US Pat. 5 424 645, 1995.
70. E. K. Paulson, R. W. Martin, and K W. Zilm, "Cross polarization, radio frequency field homogeneity, and circuit balancing in high field solid state NMR probes", *J Magn. Reson.*, 2004, **171**, 314-323..
71. X. Wu and K. Zilm, "Cross Polarization with High-Speed MAS," *J. Magn. Reson. Ser. A*, 1993, **104**, 154-163.
72. T. Gullion and J. Schaefer, in 'Advances in Magnetic Resonance', ed. W. S. Warren, Academic Press, San Diego, 1989, Vol. **13**, 57-83.
73. K. Saito, Industrial Application of Multi Nuclear Solid State NMR at High Field (16.4 T) and Super High Field (21.8 T). Presented at the 47th ENC, Asilomar, 2006.
74. I. Fischbach, K. Thieme, A. Hoffmann, M. Hehn, and Ingo Schnell, "PFG-assisted selection and suppression of ^{1}H NMR signals in the solid state under fast MAS", *J Magn. Reson.*, 2003, **165**, 102-115.
75. J. H. Chen, E. B. Sambol, P. T. Kennealey, R. B. O'Connor, P. L. DeCarolis, D. G. Cory, S. Singer, "Water Suppression Without Signal Loss in HR-MAS ^{1}H NMR of Cells and Tissues", *J Magn. Reson.*, 2004, **171**, 143-150.
76. W. E. Maas, A. Bielecki, M. Ziliox, F. H. Laukien, and D. G. Cory, "Magnetic Field Gradients in Solid State Magic Angle Spinning NMR", *J Magn. Reson.*, 1999, **141**, 29-33.
77. T. M. Barbara and C. E. Bronnimann, "Target Field Design for Magic Angle Gradient Coils", *J Magn. Reson.* 1999, **140**, 285-288,.
78. J. P. Staab, G. J. Novak, S. Kini, J. B. Spitzmesser, G. Entzminger, L. L. Holte, and F. D. Doty, "Development of a Cryo-Coil HR-MAS-PFG NMR Probe for High-field WB Magnets", presented at the 44th ENC, Savannah, 2003.
79. V. J. Bartuska, D. H. Lewis, R. B. Lewis, D. G. Dalbow, US Pat. 4 511 841, 1985.

80. H. Kovacs, D. Moskau, M. Spraul, “Cryogenically cooled probes – a leap in NMR technology”, *Mag. Reson. Spect.*, 46, 131-255, 2005.
81. R. Triebe, D. Marek “NMR Measuring Device having a Cooled Probe Head”, US Pat. 5 889 456, 1999.
82. A. Samoson, T. Tuherm, J. Past, A. Reinhold, T. Anupõld, I. Heinmaa, “New Horizons for Magic-Angle Spinning NMR”, *Topics in Current Chemistry*, 2005, **246**: 15–31, Springer-Verlag, Berlin.
83. A. S. Lipton, R.W. Heck, J. A. Sears, and P. D. Ellis, "Low temperature solid-state NMR experiments of half-integer quadrupolar nuclides: caveats and data analysis", *J Magn. Reson.*, 2004, **168**, 66-74.
84. J. L. Weil, S. L. Tan, J.S. Waugh, and D. D. Osheroff, "CP and Direct Nuclear Spin Relaxation of ^{13}C in CO at Low Temperatures," *J Magn. Reson.*, 1987, **66**, 264-73.
85. J. Zhi Hu, D. N. Rommereim, and R. A. Wind, "High-Resolution ^{1}H NMR Spectroscopy in Rat Liver Using Magic Angle Turning at a 1 Hz Spinning Rate", *Mag. Reson in Med.*, 2002, **47**, 829-836.
86. B. F. Chmelka and A. Pines, "Some Developments in NMR of Solids," *Science*, 1989, **246**, 71-77.
87. Y. Wu, B. Q. Sun, A. Pines, A. Samoson, and E. Lippmaa, "NMR Experiments with a New Double Rotor," *J. Magn. Reson.*, 1990, **89**, 297-309.
88. J. E. Readman, C. P. Grey, M Ziliox, LM Bull, A Samoson, “Comparison of the ^{17}O NMR spectra of zeolites LTA and LSX”, *Solid State NMR*, 2004, **26**, 153-159.
89. P. K. Madhu, A. Goldbourt, L. Frydman and S. Vega; "Sensitivity Enhancement of the MQMAS NMR Experiment by Fast Amplitude Modulation of the Pulses", *J. Chem. Phys.*, 2000, **112**, 2377-2391.
90. K. T. Mueller, B. Q. Sun, G. C. Chingas, J. W. Zwanziger, T. Terao, and A. Pines, "Dynamic-Angle Spinning of Quadrupolar Nuclei," *J. Magn. Reson.*, 1990, **86**, 470-87.
91. G. Zandomengehi, M. Tomaselli, J. D. van Beek, and B. H. Meier, "Manipulation of the Director in Bicellar Mesophases by (Variable Angle) Sample Spinning: A New Tool for NMR Spectroscopy," *J. Am. Chem. Soc.*, 2001, **123**, 910-913.
92. A. L. Kishore and J. H. Prestegard, “Molecular orientation and conformation of phosphatidylinositides in membrane mimetics using variable angle spinning (VAS) NMR”, *Biophys. J.*, 2003, **85**, 3848-3857.
93. T. Mizuno, T. Takegoshi, T. Terao, "Switching-Angle Sample Spinning NMR Probe with a Commercially Available 20 kHz Spinning System", *Journ. of Mag. Reson.*, 2004, **171**, 15-19.
94. S Antonijevic and G Bodenhausen, “High-Resolution NMR Spectroscopy in Solids by Truly Magic-Angle Spinning,” *Angew. Chem. Int. Ed.*, 2005, **44**, 2935-2938.
95. S. E. Ashbrook, S. Wimperis, “Satellite-transition MAS NMR of spin I = 3/2, 5/2, 7/2, and 9/2 nuclei: sensitivity, resolution, and practical implementation”, *J Magn. Reson.*, 2002, **156**, 269-281.

Biographical Sketch

F. David Doty. *b* 1950. B.A., Physics, 1972, Anderson University, IN, USA, Ph.D., 1983, Physics, University of South Carolina. Began work in NMR under Paul Ellis, 1979. President of Doty Scientific, Inc., 1982-present. Approx. 30 publications and 25 patents. Research interests include rf electronics, NMR probe technology, electromagnetism, manufacturing, turbomachinery, energy conversion cycles, ceramics engineering, acoustics, economics and religions.

Figure Captions

1. An MAS probe with a magic angle gradient coil (Doty Scientific, Inc.)
2. Supersonic sample spinner (Doty Scientific, Inc.)
3. Doubly broadband, LF/MF circuit for the outer solenoid in a triple-resonance probe.
4. Drawing of a triple-resonance MAS probe compatible with cryogenic S/N enhancement.
5. Photo of a WB SAS probe using an XC4 spinner. A fused glass-fiber light pipe is visible coming in along the reorientation axis on the near side for optical spin-rate detection. The MF/LF lead connections on the opposite side are not visible in this view, but are handled in a way similar to commutator connections in some DC motors.